Available online at www.sciencedirect.com
ScienceDirect
Trans. Nonferrous Met. Soc. China 31(2021) 92−110
Transactions of Nonferrous Metals Society of China
www.tnmsc.cn

Efficient energy absorption of functionally-graded metallic foam-filled tubes under impact loading

M. SALEHI, S. M. H. MIRBAGHERI, A. JAFARI RAMIANI

Department of Materials and Metallurgical Engineering, Amirkabir University of Technology, Tehran 15875-4413, Iran

Received 1 April 2020; accepted 11 September 2020

Abstract: The deformation behavior and crashworthiness of functionally-graded foam-filled tubes (FGFTs) under drop-weight impact loading were investigated. Closed cell aluminum, A356 alloy and zinc foams fabricated by the liquid state processing were used as axial grading fillers for the manufacture of single-layer and multilayer structures with different configurations. The results indicate that the deformation of multilayer foam filled tubes initiates from the low-strength components, and then propagates in the high-strength components through the gradual increment of stress. The use of more A356 alloy and aluminum foam layers provides greater specific energy absorption (SEA) for the graded structures, whereas the high-strength zinc foam has no positive effect on the crash performance. The progressive collapse of graded structures consisting of the aluminum and A356 alloy foams occurs in a symmetric mode under quasi-static and drop-weight impact conditions. However, the zinc foam causes a combination of symmetric and extension modes as well as greater localized deformation under dynamic loading and greater local rupture in quasi-static loading condition. The Al−A356 foam-filled tubes with a combination of the highest SEA (10 J/g) and the lowest initial peak stress (σ_{max} of 10.2 MPa) are considered as the best lightweight crashworthy structures.

Key words: functionally-graded foam-filled tube; drop-weight impact; deformation behavior; specific energy absorption; crashworthiness

1 Introduction

Metallic foams are a class of cellular materials with unique physical and mechanical properties. The most remarkable feature of a closed cell metallic foam is the ordered collapse of pores in compressive conditions, which allows for the controlled conversion of impact energy during plastic deformation up to very high strains. The foam with uniform density reveals an extended plateau region at nearly constant stress, followed by the densification at high strains [1−3]. In particular, closed cell aluminum foams have received considerable attention in the automotive industry due to their high specific strength and good energy absorption capacity [4]. Innovative concepts in the design of lightweight automobile structures have been recently sought to meet ever increasing fuel costs and stringent environmental regulations [5]. Moreover, an ideal energy absorber should maintain the maximum allowable retarding force throughout the largest possible displacement with minimum mass [6−9].

The quasi-static compressive response is normally regarded as the reference case when assessing the effects of dynamic parameters at intermediate or high loading speeds. The dynamic behavior of metallic foams at intermediate loading velocities (transitional dynamic regimes) can be studied using various test methods such as drop-weight. The literature reveals that the strain rate lies in 10^{-3}−10^{-1} and 10^{-1}−10^{3} s^{-1} for the quasi-static and transitional dynamic regimes of aluminum foams, respectively. The drop-weight impact test is more advantageous over other impact

Corresponding author: S. M. H. MIRBAGHERI; Tel: +98-21-64542961; Fax: +98-21-64542900; E-mail: smhmirbagheri@aut.ac.ir
DOI: 10.1016/S1003-6326(20)65480-2

methods due to its easy implementation, control and good repeatability. A free fall drop hammer is used for this low velocity impact evaluation method [10−14]. It is generally accepted that the strain-rate sensitivity of base material, micro-inertia, internal gas, as well as macro-inertia and structural shock wave, are key factors to affect the dynamic behavior of cellular metals. Micro-inertia is associated with cell deformation and originates from the acceleration of actual material points in the individual cell walls or struts, whereas macro-inertia appears when the axial acceleration of a macroscopic point is not zero. The walls or struts inside the cell structure actually undergo significant transverse motion under macroscopic compression due to high porosity of metallic foams, which may amplify the transverse micro-inertial force and influence the axial load resistance. The dynamic properties of a cellular metal in transitional dynamic conditions mainly arise from the microscopic strain rate sensitivity of base material and micro-inertia effect [1,13−16].

HUANG et al [17] conducted the quasi-static and split-Hopkinson pressure bar testing of closed cell aluminum foams manufactured by the direct foaming technique at nominal strain rates of 10^{-3}–10^{3} s^{-1}, respectively. They demonstrated that the dynamic failure process was dominated by the plastic bending and buckling of cell walls and tearing breakage. The resultant deformation mode and crushing response indicated the strain rate sensitivity of fabricated aluminum foams. MYERS et al [18] investigated the quasi-static and high velocity impact behavior of different aluminum alloy matrix syntactic foams at nominal strain rates of 10^{-2}–10^{3} s^{-1}, respectively. The results showed that the compressive characteristics strongly depended on the chemical composition of metallic matrix and heat treatment conditions. The aluminum alloy foams revealed a limited strain rate sensitivity in terms of structural stiffness and fracture strain. KADER et al [19] assessed the shock propagation and elastic−plastic deformation behavior of closed cell aluminium foams at loading velocities ranging from 200 to 800 m/s. The finite element modeling exhibits that the deformation initiated from the thinner/weaker cell walls in lower velocities (~200 m/s), whereas the collapse first occurred in the vicinity of impact surface at comparatively high velocities (~500 m/s). Furthermore, the pore collapse mechanism was found to be governed by the shock propagation at the velocity of about 800 m/s.

In the last decade, significant efforts have been made to use the tubular structures in the crashworthiness applications, while the energy absorption normally takes place by extensive folding and bending collapse of the tube wall in a progressive manner. For instance, aluminum tubes are connected to vehicle bumpers as crush boxes to protect the passengers under impact loading. It has been confirmed by several researchers that the mean crushing force and energy absorption capacity of thin-walled tubes can be further improved by filling them with metallic foams owing to the interaction between the foam and the tube wall. Also, a superior weight efficiency is achieved in the resulting foam-filled structures [6−9,20,21]. LINUL et al [22] explored the quasi-static crushing behavior of closed-cell aluminum foam-filled tubes at a loading speed of 10 mm/min. The results divulged that the foam filler improves the resistance of the tube to plastic deformation in a much more stable manner, leading to the enhancement of main mechanical properties up to 70%. The energy absorption of empty and foam-filled tubes in the axial loading direction was found to be up to 33 and 14 times higher than that obtained in the lateral loading direction, respectively.

DIRGANTARA et al [23] analyzed the dynamic response of aluminum foam-filled tubes. They reported that the strain rate effect of foam cores plays a significant role in the collapse behavior of foam filled structures. It was realized that the deformation mode of thin-walled tubes changed from one localized fold to multiple propagating folds caused by the interaction between the foam core and the square tube, leading to the increment of mean crushing force and energy absorption. It is worthwhile noting that the interaction component relies on the relative stiffness of the interface and the penetration resistance of the foam layer adjacent to the tube. In fact, the energy absorbing ability of foam-filled structures is found to be highly dependent on the foam density in a way that increasing the foam density would ensure the enhancement of total energy absorption, although it is not always the case for the specific energy absorption (SEA). In other words, the uniform foam fillers cause to improve the crash

features of thin-walled members to a considerable extent and may not exert the maximum capacity of materials to meet the requirements of vehicular lightweighting. So, there is an urgent need to develop new structural configurations with nonuniform distributions of materials for optimizing the crashworthiness [5,24,25].

The newest class of cellular materials consists of functionally-graded foams (FGFs), in which the properties vary gradually or layer by layer as dimension changes [26]. It has already been shown that the FGFs are suitable candidates for tailoring multifunctional behaviors and providing improved energy absorption ability over the conventional uniform-density foams [27]. There have been great attempts in the recent years to look into the possibility of designing FGFs for different applications. HE et al [28] carried out the quasi-static experiments and numerical simulations of continuously graded aluminum foams prepared by the direct foaming route coupled with the solidification process. They demonstrated that the lower TiH_2 content of foaming agent and shorter holding time resulted in a greater density gradient in aluminum foam. It was shown that the progressive collapse of graded foams initiated from lower density regions and extended to higher density regions.

The FGFs with multilayers are very attractive in terms of energy absorption and passive safety protection since they can dissipate the impact kinetic energy in a controlled manner [29−31]. KOOHBOR and KIDANE [32] examined the quasi-static crushing and energy absorption capability of layered polymeric foams at nominal strain rate of 1.3×10^{-3} s^{-1}. The results indicated that the stepwise increase in the global stress−strain curves of FGFs was associated with stress levels at which each individual layer reached its elastic limit and yielded. It was noticed that the discretely graded foams exhibited superior energy absorption performance compared with the uniform foams at low stress levels, whereas an opposite trend was observed at high stress levels. MAHEO and VIOT [33] suggested that the ascending density gradient allows for a progressive absorption of energy without involving a plateau stage in layered polymeric foams. MOVAHEDI et al [34] performed the quasi-static compression test of double-layer metal matrix syntactic foams composed of ZA27 alloy matrix with embedded perlite and activated carbon filler particles. They reported that the deformation of FGFs at low strain resembled the crushing response of perlite metal syntactic foam, whereas the subsequent failure of activated carbon metal syntactic foam happened at high strains. The proposed FGFs showed higher energy absorption efficiency with respect to the uniform counterparts.

HANGAI et al [35−37] developed the double-layer FGFs with various aluminum base materials, including A1050/A6061, Al/AC4CH and Al/ADC12, by the precursor foaming process. It was found that the FGFs exhibited multiple mechanical properties and higher functionality compared to the uniform foams when subjected to quasi-static and drop-weight loading. They deduced that the weak layer with higher porosity started to deform firstly at lower plateau force, and then the compaction occurred in the strong layer with lower porosity at higher plateau force, regardless of the location of foam layers. ZHANG et al [38] explored the dynamic response and energy absorption of double-layer aluminum foams using the split Hopkinson pressure bar. The experimental results divulged that the graded foams were compacted layer by layer, and the dynamic crushing initiated from the soft layer with higher porosity at low impact velocities of about 15 m/s. The mesoscopic investigations implied that the stress−strain curves of FGFs with a negative porosity arrangement had two plateau stages at high impact velocities of about 300 m/s, whereas the stress plateau decreased gradually in FGFs with a positive porosity arrangement, i.e., the collapse and the fracture of cell walls first happened at the impact end under high velocity impact loading. It was concluded that the double-layer foams presented better protection capability than the uniform foams, and the energy absorption was improved significantly with the increase in loading speed from 30 to 300 m/s.

Recently, several studies in the literature have been devoted to the finite element simulation of functionally-graded foam-filled tubes (FGFTs), including a discrete form of foam core defined through certain density gradient functions, and confirmed their superior crashworthiness to the uniform counterparts [4,7,39−42]. To the best knowledge of the authors, a few experimental works are available on the dynamic properties and

energy absorption of FGFTs containing various foam materials. The current study expands upon our previous article [43] and presents novel discretely graded foam-filled tubes, including one, two, three or four layers of zinc foam, aluminum foam and A356 alloy foam in different configurations. The authors aim to investigate the drop-weight impact behavior of FGFTs and to introduce the structures with the best crash features. The role of foam material and structure in the dynamic response of FGFTs is analyzed using the SEM observations. The effect of density, material, number and sequence of foam layers on the impact properties and SEA of graded structures is surveyed. Also, the comparison of deformation pattern between dynamic and compressive conditions is fulfilled by conducting some limited quasi-static experiments of FGFTs.

2 Experimental

2.1 Manufacture of metallic foams

Closed cell metallic foams were fabricated by the liquid state processing using titanium hydride (TiH_2) as the foaming agent. Pure aluminum, zinc and A356 alloy with the chemical compositions and mechanical properties presented in Table 1 were used to produce three distinct metallic foams. For the manufacture of aluminum foam, as schematically illustrated in Fig. 1, firstly, the pure aluminum was melted in a carbon steel crucible and maintained at 730 °C. Next, 2 wt.% of Ca granules, acting as a thickening agent, were added into the melt at a stirring speed of 800 r/min for 8 min. Afterwards, 0.75 wt.% of TiH_2 powder, which serves as a blowing agent by releasing hydrogen gas in the hot viscous liquid, was dispersed at a stirring speed of 1700 r/min for 80 s. Then, the melt was poured into a cubic steel mold and maintained in an electric furnace to allow for foam formation at 680 °C in 3 min. Once the foaming was completed, the crucible was taken out and cooled down in air to solidify the foam and prevent hydrogen from escaping. The same procedures were performed for the production of alloy and zinc foams, except that the foaming temperatures were set to be 640 and 500 °C, respectively. Besides, more amount of TiH_2 (1.2 wt.%) and longer time of the foaming process (12 min) were employed in the zinc foaming process since the decomposition of TiH_2 occurred more slowly in the pure zinc with lower melting point compared to aluminum alloys. It should also be noted that 3 wt.% aluminum was added into the zinc melt to achieve a homogeneous structure with increasing liquid viscosity [43,44]. Eventually, the aluminum, A356 alloy and zinc foams with the densities of 0.2, 0.3 and 2.4 g/cm^3 were prepared, respectively.

Table 1 Chemical composition and mechanical properties of raw materials for manufacturing metallic foams

Material	Chemical composition/wt.%	ρ/(g·cm^{-3})	Elongation/%	σ_y/MPa	σ_b/MPa
Aluminum	Al 99.68	2.71	18	70	102
A356 alloy	Si 7.31 + Mg 0.29 + Cu 0.04 + Fe 0.12 + Al Bal.	2.56	4.7	92	181
Zinc	Zn 99.44	7.14	–	31	–

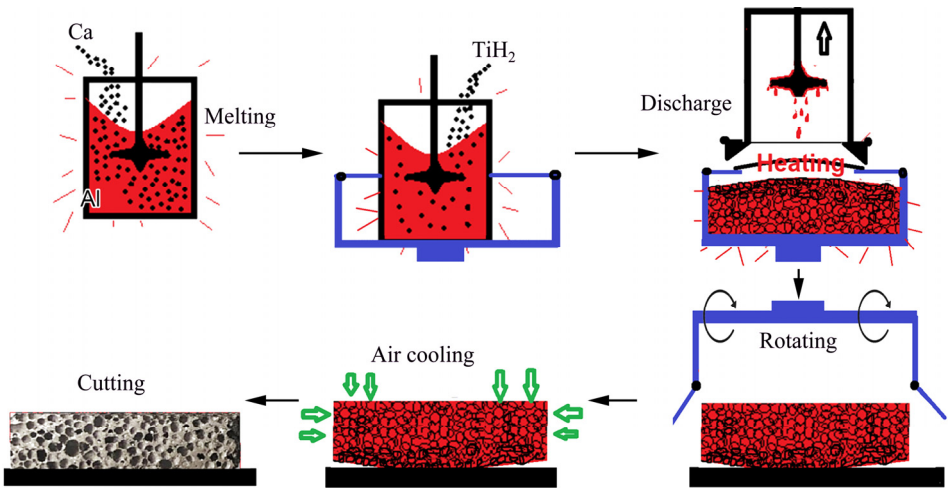

Fig. 1 Schematic illustration of aluminum foam fabrication by liquid state processing

2.2 Preparation of FGFTs

The design of FGFTs was implemented considering variations in material, number and arrangement of metallic foam layers. According to Table 2, the multilayer structures were categorized into four groups with the same foam materials, where the Al, A356, Zn and FFT were used for addressing the aluminum, A356, zinc and foam-filled tube, respectively. For instance, Al−A356−Zn FFT represents a square tube filled with three layers of aluminum foam (top layer), A356 alloy foam (middle layer) and zinc foam (bottom layer) of the same length. It should be noticed that the double and triple layer FFTs were composed of dissimilar foam materials, whereas the fillers of quad layer ones were configured using two foam materials. Besides, the uniform foam filled tubes of Al FFT, A356 FFT and Zn FFT were fabricated and compared with multilayer ones. For the manufacture of single, double, triple and quad layer structures based on various configurations presented in Table 2, rectangular pieces of metallic foams with the cross section of 18 mm × 18 mm and thickness of 60, 30, 20 and 15 mm were prepared to serve as the fillers, respectively. The square aluminum extrusions with outer cross section of 20 mm × 20 mm and thickness of 1 mm were cut into the tubes with 60 mm in length. The designed samples were finally produced by fitting the foam fillers into the tubes along the axial direction without any adhesive materials. Figure 2 shows the schematic layer arrangements and manufacture of FGFTs.

2.3 Mechanical and structural characterization

Low velocity impact tests were performed on the three metallic foams with the dimensions of 20 mm × 20 mm × 60 mm, and the FGFTs mentioned in Section 2.2. So, a total number of 26 dynamic experiments were conducted with a drop-weight testing machine according to ISO 17340 standard [45]. A 20 kg weight fell freely from the height of 1.5 m, causing the release of kinetic energy and collapse of the structures. The concurrent impact energy and velocity are 294 J and 5.4 m/s, respectively. The engineering stress−strain data were determined through the load−displacement measurements, taking account of initial dimensions. Moreover, the quasi-static compressive response of metallic foams and some FGFTs was examined by an INSTRON universal testing machine (Model 8502) with a load capacity of 250 kN at a loading velocity of 12 mm/min (nominal strain rate of 3.3×10^{-3} s^{-1}) according to ISO 13314 standard [46]. The total crushing displacement was set to be approximately 45 mm (~0.75 strain), and the collapse process was photographed during the quasi-static compaction. The microstructure of metallic foams was studied using the scanning electron microscopy/ energy dispersive X-ray spectroscopy (SEM/EDS) analysis.

The relative density, as the ratio be the foam apparent density (ρ_f) to the base material density (ρ_s), is the main structural parameter that determines the energy absorption capability of cellular structures. The ρ_f and ρ_s of graded fillers in the FGFTs with various foam materials were calculated by the following equations [32,47,48]:

$$\rho_f = \sum_{i=1}^{N} \rho_{f,i} / N \quad (1)$$

Table 2 Design of layer configurations in various categories of multilayer foam-filled tubes

Al−A356−Zn foams	Al−A356 foams	Al−Zn foams	A356−Zn foams
Al−A356−Zn FFT	Al−A356 FFT	Al−Zn FFT	A356−Zn FFT
Zn−A356−Al FFT	A356−Al FFT	Zn−Al FT	Zn−A356 FFT
Al−Zn−A356 FFT	Al−Al−A356−A356 FFT	Al−Al−Zn−Zn FFT	A356−A356−Zn−Zn FFT
A356−Zn−Al FFT	A356−A356−Al−Al FFT	Zn−Zn−Al−Al FFT	Zn−Zn−A356−A356 FFT
A356−Al−Zn FFT	Al−A356−Al−A356 FFT	Al−Zn−Al−Zn FFT	A356−Zn−A356−Zn FFT
Zn−Al−A356 FFT	A356−Al−A356−Al FFT	Zn−Al−Zn−Al FFT	Zn−A356−Zn−A356 FFT
	Al−A356−A356−Al FFT	Al−Zn−Zn−Al FFT	A356−Zn−Zn−A356 FFT
	A356−Al−Al−A356 FFT	Zn−Al−Al−Zn FFT	Zn−A356−A356−Zn FFT

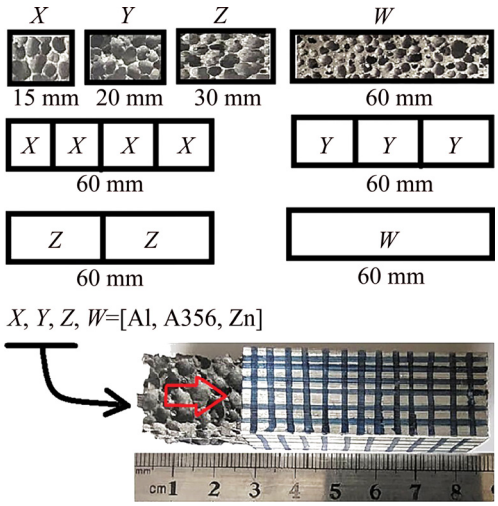

Fig. 2 Schematic layer arrangements and manufacture of FGFTs

$$\rho_s=\sum_{i=1}^{N}\rho_{s,i}\Big/N \tag{2}$$

where $\rho_{f,i}$ and $\rho_{s,i}$ denote the foam apparent density and the base material density of each foam material, respectively. Also, N is the number of foam materials in a graded structure. So, the relative densities of 0.1, 0.27, 0.28 and 0.23 were provided for graded foam fillers of the Al−A356, Al−Zn, A356−Zn and Al−A356−Zn multilayer categories, respectively.

The impact performance of FGFTs was evaluated in terms of the specific energy absorption (SEA, A), plateau stress (σ_{mean}) and initial peak stress (σ_{max}) as the main crashworthiness indicators. Generally, the SEA is regarded as the key factor to select the efficient lightweight energy absorbing structures and defined using the force−displacement curves, as follows [49−53]:

$$A=\frac{\int_0^{x_t}F(x)\mathrm{d}x}{m} \tag{3}$$

where x_t is the total crushing distance, and m is the mass. Meanwhile, the σ_{mean} is an effective indicator to assess the collapse resistance of a crashworthy device and given as follows [39,54,55]:

$$\sigma_{mean}=\frac{\int_{\varepsilon_{max}}^{\varepsilon_t}\sigma(\varepsilon)\mathrm{d}s}{\varepsilon_t-\varepsilon_{max}} \tag{4}$$

where ε_{max} and ε_t are the initial peak strain and total crushing strain, respectively. The σ_{max} is another critical indicator to reflect the deceleration under impact, while the lower the σ_{max}, the better the protection of the entire structure [49,51,56].

3 Results and discussion

3.1 Structure of metallic foams

Closed cell foams consist of numerous pores, cell walls (cell faces) and cell struts (plateau borders) [57,58]. Figure 3 shows the lognormal pore size distribution of fabricated foams fitted through the image analysis of representative areas with 50 mm in diameter. The cell morphology of metallic foams seems to be almost heterogenous owing to large frequency variations within a wide range of pore size. The average pore size is measured to be 1.22, 1.10 and 0.74 mm in the aluminum, A356 alloy and zinc foams, respectively.

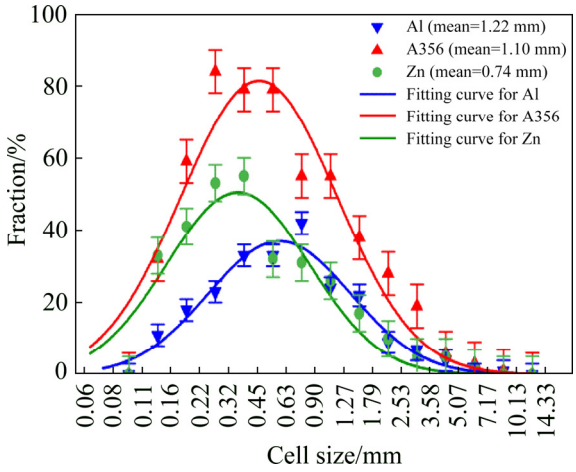

Fig. 3 Pore size distribution of metallic foams

It is generally accepted that the compressive behavior of metallic foams is mainly governed by the cell wall material and microstructure. The SEM images and EDS results of aluminum, A356 alloy and zinc foams are illustrated in Figs. 4, 5 and 6, respectively. Figure 4(a) indicates the pore size of aluminum foam. Also, the cell strut microstructure reveals several white needles in the aluminum matrix, as seen in Fig. 4(b). Based on EDS analysis given in Fig. 4(c), Zone A can be characterized as complex $FeAl_2$ or Fe_2Al_5 intermetallic phase, originating from the steel stirrer. Meanwhile, Zone B denotes the aluminum matrix regarding Fig. 4(d). The apparent peaks of calcium, silicon and titanium are detected in the EDS results of aluminum foam. The structure of hypo eutectic A356 alloy consists of a eutectic mixture of needle-shaped silicon

particles dispersed in the interdendritic regions of an aluminum-rich α solid solution (1.65 wt.% silicon) and a pre-eutectic α solid solution [59−61]. Figures 5(a, b) show the formation of a fine lamellar phase in the cell wall microstructure of A356 foam. According to Fig. 5(c), Zone A is specified as the α solid solution, while the eutectic (α-Si) network appears in Zone B considering Fig. 5(d). The peaks of calcium, iron, copper, magnesium and titanium are also found in the EDS results of A356 foam. In the case of zinc foam, the addition of aluminum into the melt leads

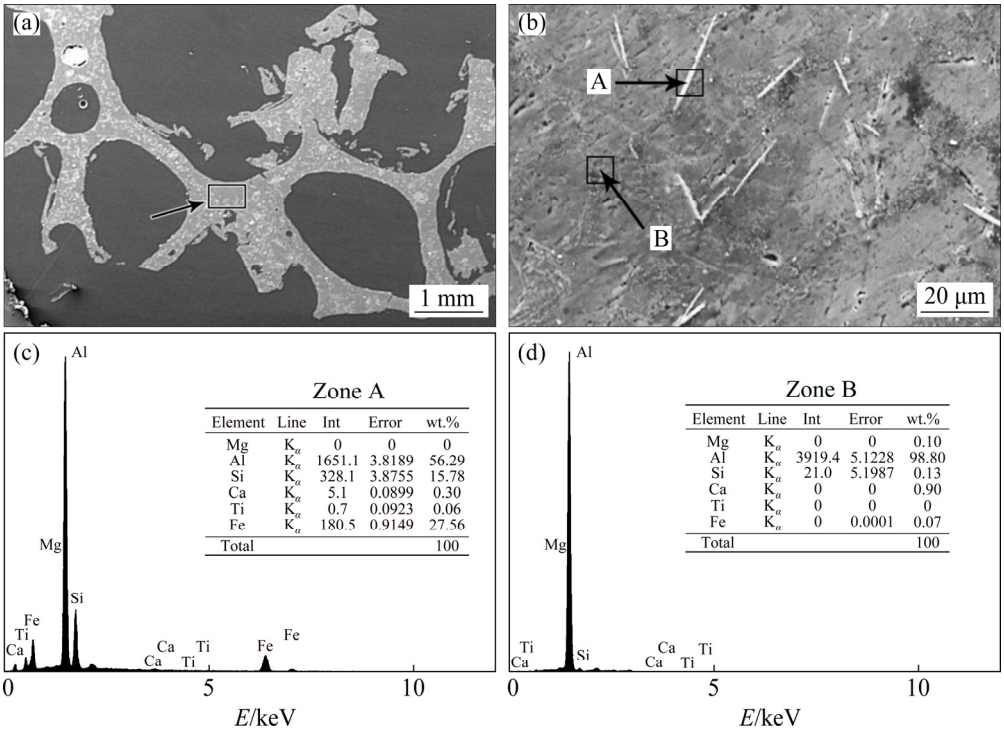

Fig. 4 Microstructures of aluminum foam (a, b), and EDS analyses of Zone A (c) and Zone B (d)

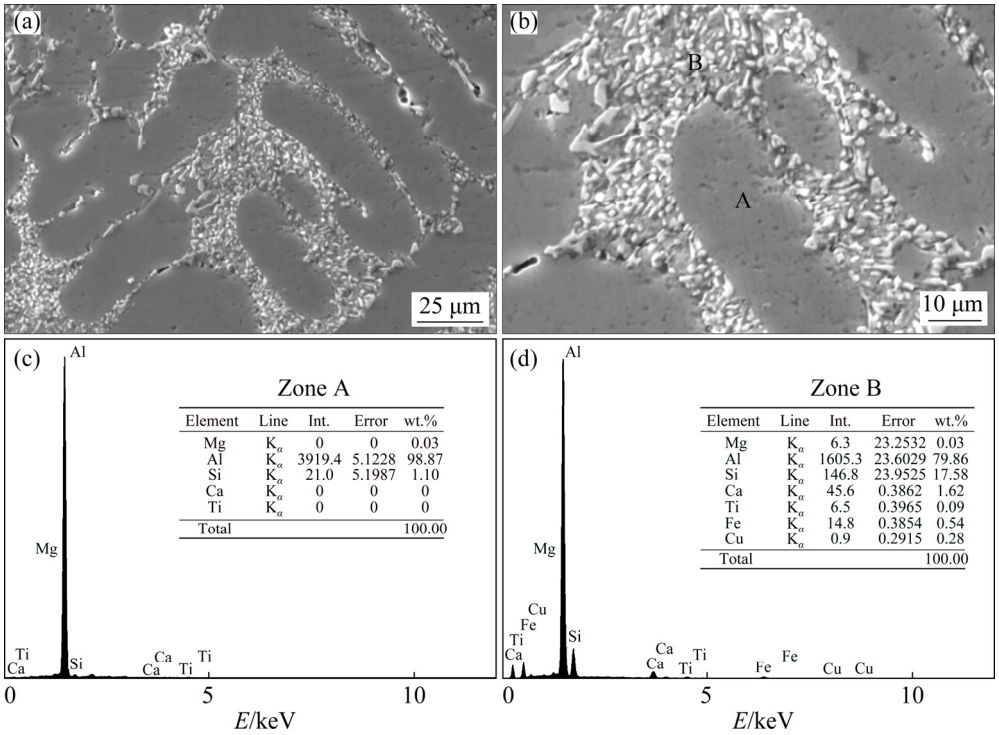

Fig. 5 Microstructures of A356 alloy foam (a, b) and EDS analyses of Zone A (c) and Zone B (d)

to the development of a pre-eutectoid η solid solution (0.7 wt.% aluminum) and a eutectoid (η+α) phase. Figures 6(a, b) imply that a lamellar eutectoid structure exists in the cell wall microstructure of zinc foam. The EDS results of Zn foam given in Fig. 6(c) suggest that Zone A is zinc matrix containing a small amount of aluminum and calcium. The peaks of magnesium, calcium and copper are obvious in the EDS analysis of zinc foam. As a consequence, the cell wall structure of aluminum foam mostly consists of the ductile FCC matrix [16,61−63]. By comparison, the strong lamellar phases propagate in the cell walls of A356 alloy and zinc foams seem to play a dominant role in their crash performance.

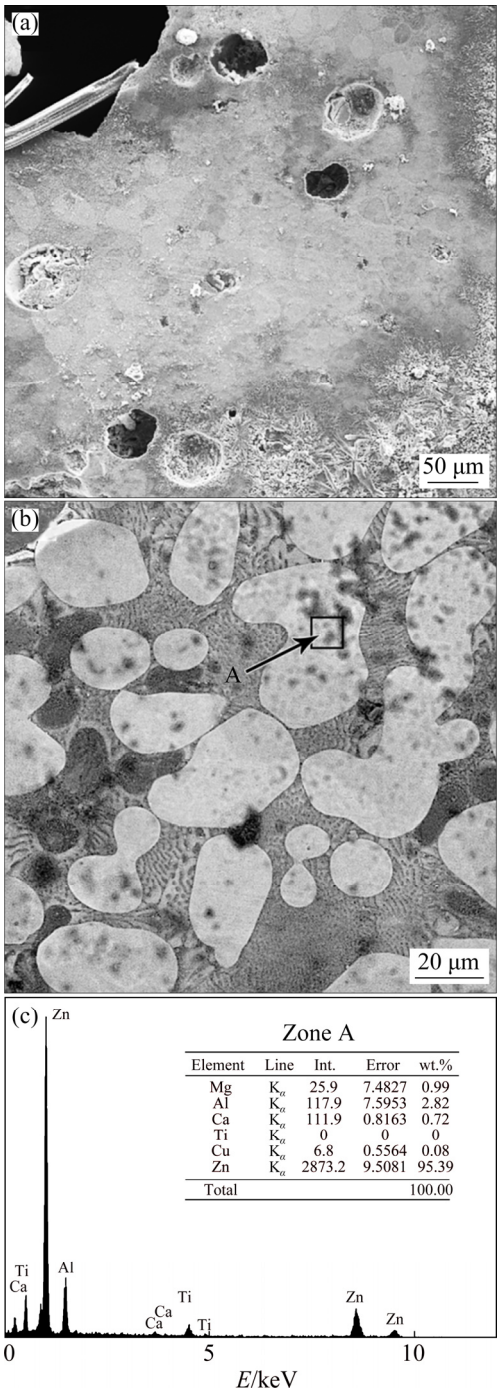

Fig. 6 Microstructures of zinc foam (a, b) and EDS analysis of Zone A (c)

3.2 Drop-weight impact behavior

Figure 7 shows the dynamic response of uniform foams and foam-filled tubes. The stress−strain curves of metallic foams reveal the three distinct regions: (1) Initial elastic region is characterized by elastic deflection of cell walls and increasing the stress in a linear fashion for a small increment of strain; (2) The linear region terminates into a local maximum stress (σ_{max}) as an indication of the yield strength, followed by a stress relaxation to an extensive plateau region, wherein the buckling, stretching and cracking of the cell walls occur inside the localization bands; (3) The collapsed cells are compacted, and the material acts as a solid material during rapid hardening in the densification region. It is worthwhile noting that obvious stress fluctuations appear in the plateau stage of metallic foams associated with the anisotropic cell morphology and sequential crushing of deformation bands. It seems that the zinc foam has higher-degree fluctuations, representing its larger structural inhomogeneity with respect to the aluminum and A356 alloy foams [2,8,14,19]. Meanwhile, the dynamic compaction of single layer foam-filled tubes exhibit almost similar trend to that observed in the metallic foams. However, inserting a foam filler into the thin-walled tube causes an interaction between the foam and tube wall and, thereby, a

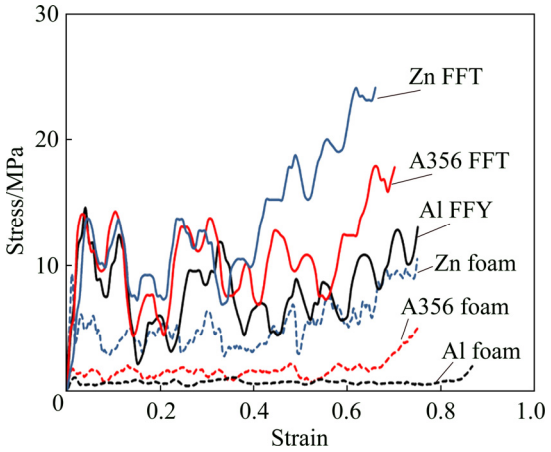

Fig. 7 Stress−strain curves of uniform foams and foam-filled tubes under impact loading

drastic increase in stress levels. The σ_{max} is followed by a severe drop in stress and successive fluctuations. During the collapse process, a square folding is created in the weakest region after the structure starts to yield. Then, the stress reduces to lower values, indicating the tube wall bending. When the first folding is impacted, the stress raises again and the second folding forms next to the first one. The progressive deformation mode continues and results in a zigzag portion of stress−strain curve. So, it is expected that a direct relation exists between the degree of fluctuations and the number of foldings in foam-filled tubes [15,23,64].

Figure 8 gives the σ_{mean} and σ_{max} values of uniform foams and foam-filled tubes. The zinc foam with much greater density presents higher stress levels and crushing resistance in contrast to the A356 alloy and aluminum foams. The reason is that the foam with higher density has more cell walls bearing permanent deformation and, thereby, higher resistance to compression loads. Further, the A356 alloy cell wall material has larger strength with respect to the aluminum and zinc foams regarding Table 1, which can be attributed to the eutectic needle-shaped silicon formed in the interdendritic regions. So, despite almost identical densities, the σ_{max} and σ_{mean} of A356 alloy foam is found to be higher than that of the aluminum foam. In fact, the impact properties of metallic foams are primarily governed by the density, and then by the foam material, as confirmed in Refs. [1,59,65,66]. It should be noticed that the interaction component in the foam-filled structures relies on the relative stiffness of the interface and the penetration resistance of the foam layer adjacent to the tube.

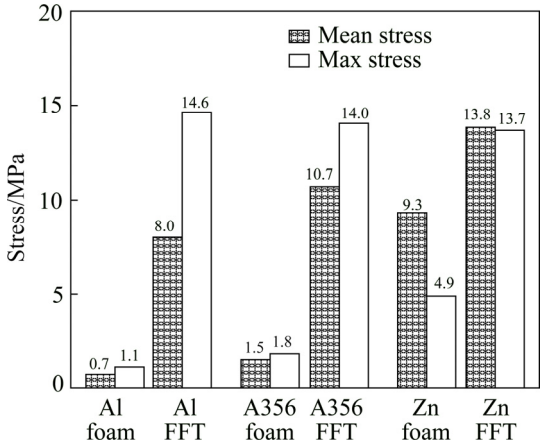

Fig. 8 σ_{mean} and σ_{max} values of uniform foams and foam-filled tubes

Therefore, the Zn FFT shows the highest σ_{mean} among the single-layer FFTs, followed by the A356 FFT [41,49,67]. Nevertheless, the σ_{max} of single-layer structures is approximately the same owing to noticeable σ_{max} of the empty tube.

In order to evaluate the influence of design parameters on the impact characteristics of FGFTs, Fig. 9 exhibits the representative stress−strain curves of various categories of multilayer structures. The impact responses of multilayer FFTs with the reverse order of grading layers are nearly similar. Overall, the arrangement of foam layers has no significant effect on the dynamic features of graded structures. In addition, a stepwise increment of stress appears in the crushing curves of multilayer structures, despite relatively steady deformation of single-layer ones. It seems that the collapse first occurs in the weak layers with lower strength, and then propagates in the strong layers with higher strength at large strains. In other words, high strength components are not expected to experience plastic deformation when the stress in the structure is below the σ_{max} of corresponding single-layer structures. Figure 9 suggests that the use of zinc foam filler in the graded structures leads to a dramatic rise of stress and a decrease in total deformation. Consequently, the drop-weight impact properties of FGFTs are primarily governed by the density and material of foam fillers [32−38,42,43]. It is also deduced that the sharper increment of the stress plateau happens during the stepwise hardening with increasing the number of foam layers in each category, particularly in the Al−Zn FFTs. This can be attributed to the stress transmission through more material interfaces [68].

Generally, high σ_{mean} and low σ_{max} are desired in the design of energy absorbers with superior protection. Figure 10 shows the average σ_{mean} and σ_{max} by varying the foam materials of multilayer structures. The maximum σ_{mean} and the minimum σ_{max} are achieved in the A356–Zn FFTs (18.9 MPa) and Al–A356 FFTs (12.5 MPa), respectively. Regarding Figs. 8 and 10, the multilayer structures, particularly the A356–Zn FFTs, have larger average amounts of σ_{mean} and σ_{max} compared with the constituting single-layer structures. It is worthwhile noting that the Al−A356 FFTs reveal higher σ_{mean} and lower σ_{max} with respect to the single-layer Al FFT and A356 FFT and, thereby, the best dynamic performance among the graded structures. The

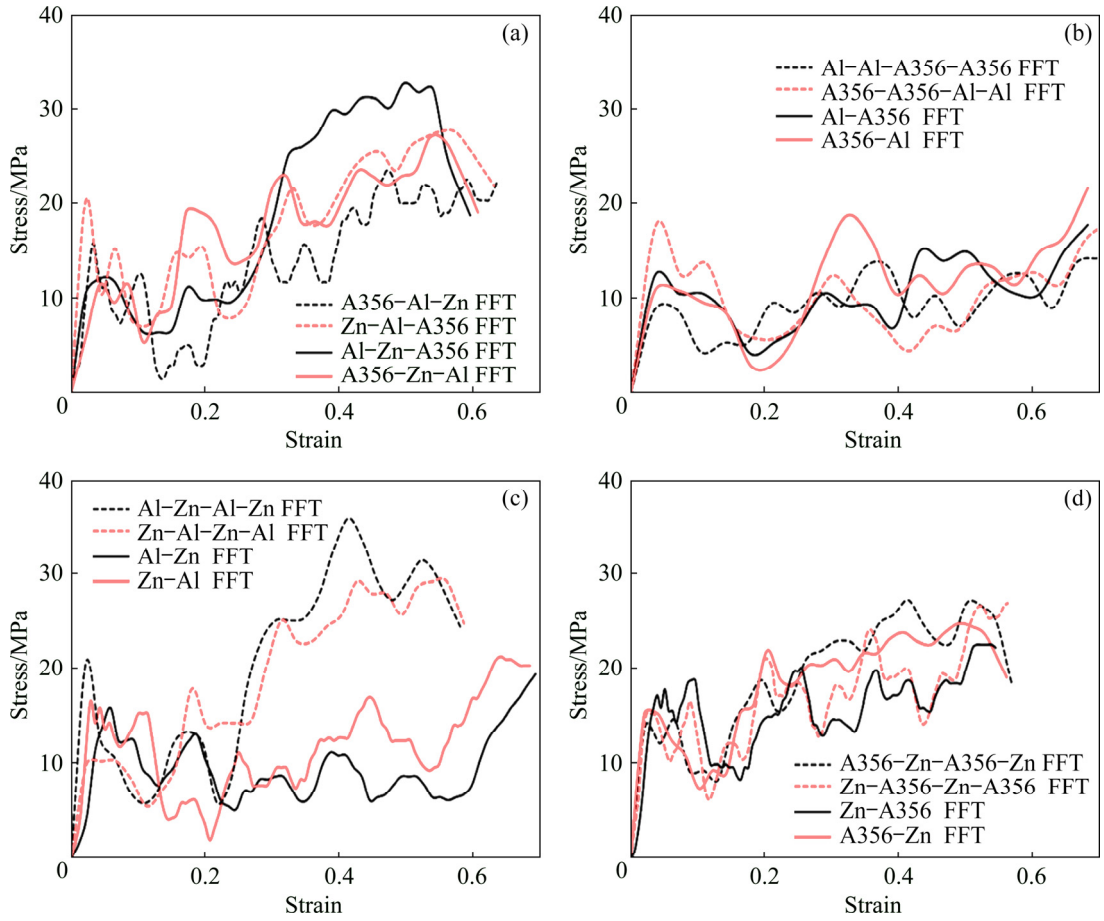

Fig. 9 Stress−strain curves of various multilayer FFTs under impact loading: (a) Triple layer; (b) Al−A356; (c) Al−Zn; (d) A356−Zn

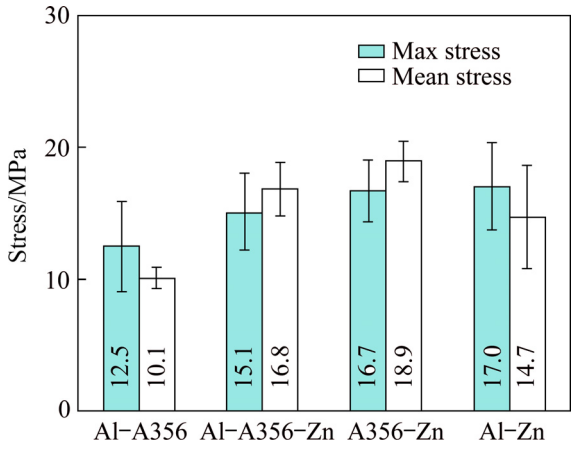

Fig. 10 Average σ_{mean} and σ_{max} of various categories of multilayer structures

average σ_{mean} and σ_{max} of graded structures are significantly affected by the volume fraction of zinc foam due to its much greater density relative to the A356 alloy and aluminum foams [69,70]. As a consequence, the dynamic features can be controlled by varying the density, material and number of foam layers in the design of FGFTs.

The deformation behavior under dynamic loading seems to differ from the quasi-static condition in two characteristic ways, mainly associated with the increase in localized deformation and possible introduction of global bending effects. Figure 11 illustrates the failure modes of some multilayer FFTs from different categories after drop-weight impact testing by preparing the longitudinal cross sections. Generally, four compact lobes develop progressively in the Al−A356 FFTs, while the collapse mode is characterized to be symmetric by generating the lobes moving alternately inwards and outwards. Also, irregular folding or localized deformation occurs by introducing the zinc foam into multilayer structures. In other words, an extension mode appears in regions containing the high-strength zinc foam, where the lobes move totally outwards [23,49,67,71]. Therefore, the Al−Zn, A356−Zn and Al−A356−Zn FFTs reveal a combination of symmetric and extension modes by creating three local lobes. In fact, despite the high

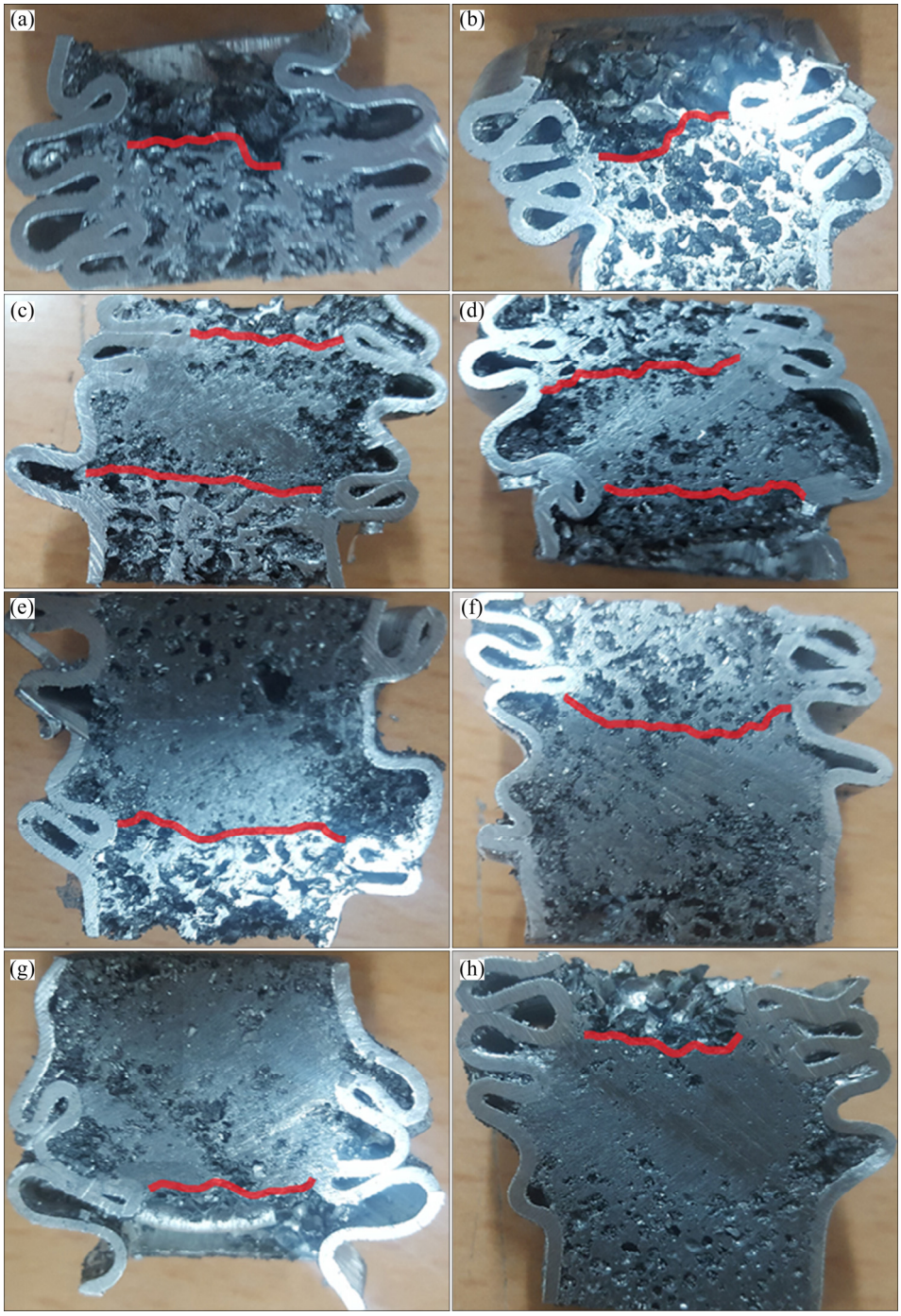

Fig. 11 Failure modes of some multilayer structures under impact testing: (a) A356−A356−Al−Al FFT; (b) Al−Al−A356−A356 FFT; (c) Al−Zn−A356 FFT; (d) A356−Zn−Al FFT; (e) Zn−Zn−A356−A356 FFT; (f) A356−A356−Zn−Zn FFT; (g) Zn−Zn−Al−Al FFT; (h) Al−Al−Zn−Zn FFT

cohesion of aluminum and A356 alloy foams with the tube wall, the zinc foam provides high constraint when the tube wall buckles, tolerates small deformation, and may even be detached from the tube in some cases. So, the zinc foam layers are conjectured to transfer most of the kinetic energy to the adjacent foam layers and make no effective contribution to the energy absorption capability of FGFTs.

The quantitative comparison of plastic deformation between the metallic foams can be fulfilled by measuring their final length in the multilayer FFTs based on materials interfaces marked by red lines in Fig. 11. The total length is

related to the length of constituting foam materials, as follows [32−37]:

$$l_0=nl_{0,i} \text{ and } l_t=\sum_{i=1}^{n} l_i \tag{5}$$

where n is the number of foam materials, l_0 is the initial length and l_t is the final length of multilayer structure. Also, $l_{0,i}$ and l_i denote the initial length and the final length of each foam material, respectively.

The strain of individual foams is measured using the following equation:

$$\varepsilon_i=1-\frac{l_i}{l_{0,i}}=1-\frac{nl_i}{l_0} \tag{6}$$

where ε_i is the strain of foam material i. Therefore, the total strain (ε_t) can be defined according to the following equation:

$$\frac{l_t}{l_0}=\frac{\sum_{i=1}^{n} l_i}{l_0}=\frac{\sum_{i=1}^{n}(1-\varepsilon_i)}{n}=\frac{n-\sum_{i=1}^{n}\varepsilon_i}{n}\rightarrow \varepsilon_t=1-\frac{l_t}{l_0}=\frac{\sum_{i=1}^{n}\varepsilon_i}{n} \tag{7}$$

The final length of constituting foams in the multilayer structures is measured regarding materials interfaces, and the strain is calculated based on Eq. (6). Then, the mean strain of each foam material and the mean total strain for various categories of multilayer structures are obtained, as presented in Fig. 12. On average, the Al−A356 FFTs experience the maximum total strain among the multilayer FFTs, as expected. Moreover, the relatively constant strains of about 0.8, 0.6 and 0.5 are achieved in the aluminum, A356 alloy and zinc foams in multilayer structures, respectively. The apparent density and cell wall material and structure seem to be responsible for different deformation abilities of metallic foams. The low density and ductile FCC structure of the aluminum foam lead to the largest mean strain. Conversely, the high density and formation of hard eutectoid phase in the brittle HCP matrix provide the smallest mean strain for the zinc foam [62]. It is worthwhile noting that the A356 alloy foam containing a considerable amount of brittle needle-shaped silicon in its cell walls and struts shows higher collapse resistance in contrast to the aluminum foam, despite the relatively similar densities. Therefore, the deformation extent of individual metallic foams in multilayer structures is found to be simultaneously dependent on the foam density and structure.

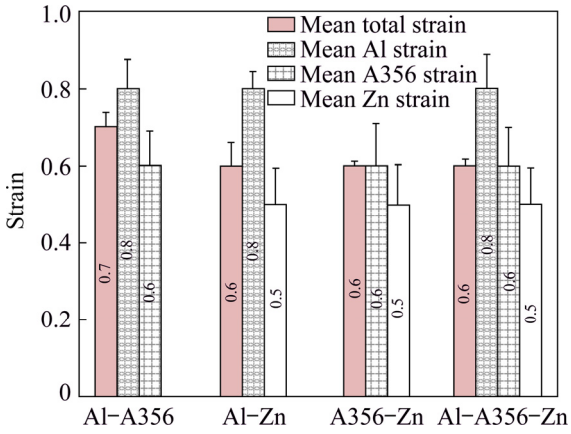

Fig. 12 Mean strain of metallic foams and mean total strain for various categories of multilayer structures

A comparison between the impact and compressive behavior of FGFTs is accomplished by providing the quasi-static response of some representative single-, double- and triple-layer FFTs, as illustrated in Fig. 13. The stress−strain curves of uniform foam filled tubes follow almost similar trends to those obtained under impact loading, as seen in Figs. 13(a, b, c). The primal elastic region is followed by yielding and plastic hardening to σ_{max}, then by a plateau region, and eventually, by a dramatic hardening in the densification stage. It should be noticed that higher-degree fluctuations exist in the dynamic condition probably due to the instability of impact testing. Besides, too much density difference between the zinc foam and the aluminum or A356 alloy foams results in higher σ_{mean} of the Zn FFT (28.2 MPa) compared to the Al FFT and A356 FFT (9.9 and 11.5 MPa, respectively). The collapse of single-layer FFTs initiates from the clamping support. Similar to what observed in the dynamic condition, the Al FFT and A356 FFT exhibit the symmetric failure mode, and an extension mode happens in the Zn FFT. Further, the high strength zinc foam filler may cause tearing of the tube corners owing to the excessive tensile strain, leading to the evidence of local rupture (breaking of corner regions) during the last stages of deformation [23,49].

It seems that the multilayer structures reveal significant compressive features depending on the material and number of foam layers. The stress−strain curves of double-layer FFTs include two distinct plateau regions, as shown in Figs. 13(d, e, f).

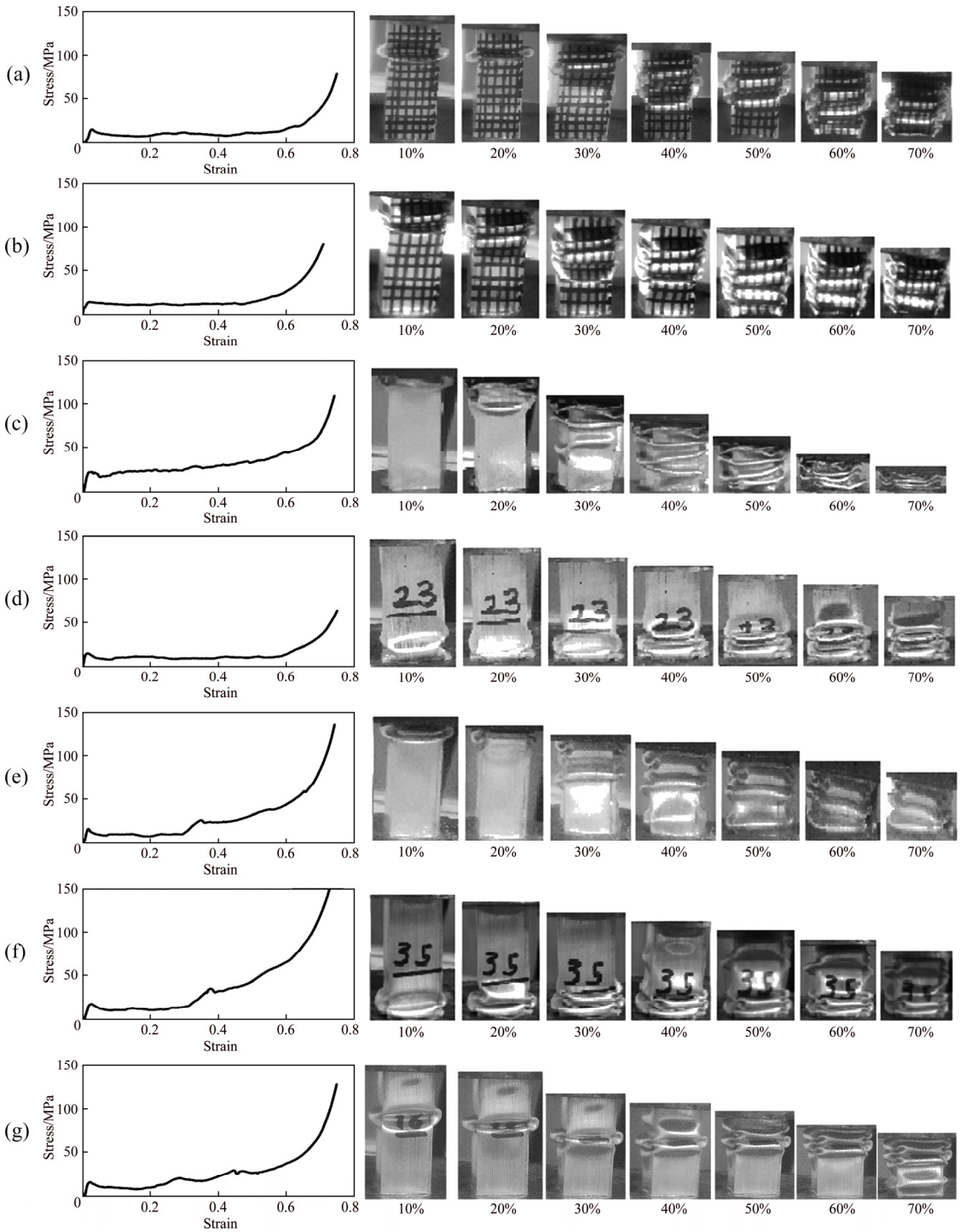

Fig. 13 Stress−strain curves and sequential pictures of Al FFT (a), A356 FFT (b), Zn FFT (c), A356−Al FFT (d), Al−Zn FFT (e), Zn−A356 FFT (f) and A356−Al−Zn FFT (g) under quasi-static loading

The sequential images indicate that the first plateau region is associated with stable deformation of the lower strength component, while the second plateau region corresponds to plastic buckling of the higher-strength component. According to Fig. 13(g), the crushing curve of triple-layer A356−Al−Zn FFT consists of three distinct plateau regions, which can be attributed to successive deformation of the aluminum, A356 alloy and zinc foam layers, respectively. It is also found that the stress in each plateau stage of multilayer structures is near to the σ_{mean} of corresponding single-layer counterparts. In addition, the occurrence of irregular folding, i.e., the combination of symmetric mode in the

aluminum or A356 alloy foam layers and extension mode in the zinc foam layers is consistent with the impact results. As a consequence, the use of zinc foam in the graded structures causes the local deformation in the dynamic condition and local rupture in the quasi-static condition [41,71].

3.3 Crashworthiness assessment

The energy absorption capacity is of particular importance to the design of protective structures. Figure 14 shows the absorbed energy against stress during plastic deformation of some FGFTs. Figure 14(a) indicates that the single-layer FFTs exhibit a steady absorption of energy within a narrow stress range. By comparison, the multilayer FFTs tend to gradually absorb energy through the successive collapse of individual foam layers with different materials and densities in a wider stress range, as seen in Figs. 14(b, c, d). So, the multilayer structures seem to be the most adapted to impact conditions when a stepwise increasing energy absorption is desired [32,33].

The SEA of FGFTs is calculated based on Eq. (3) and reported in Fig. 15. It is generally accepted that an enormous increase in the density may reduce the SEA [32,33,47,48]. In fact, low density and great inherent strength of the A356 foam, originating from the needle-shaped silicon in its microstructure, provides the most SEA of 9.9 J/g for the A356 FFT among the single-layer FFTs. On the contrary, high density and brittle HCP matrix of the zinc foam are responsible for the lowest SEA of 3.6 J/g in the Zn FFT. The Al FFT with the ductile FCC matrix and low density also reveals a comparatively high SEA of 8.9 J/g. Therefore, the SEA of uniform FFTs is mainly dominated by the density and the cell wall structure of the foam filler. The maximum SEA of 10.9 J/g is achieved in the double-layer A356−Al FFT, which is 10% and 22% higher than that of the single layer A356 FFT and Al FFT counterparts, respectively. Generally, the multilayer Al−A356 FFT exhibits higher SEA values with respect to the A356 FFT and Al FFT, probably attributed to gradual increase in the stress

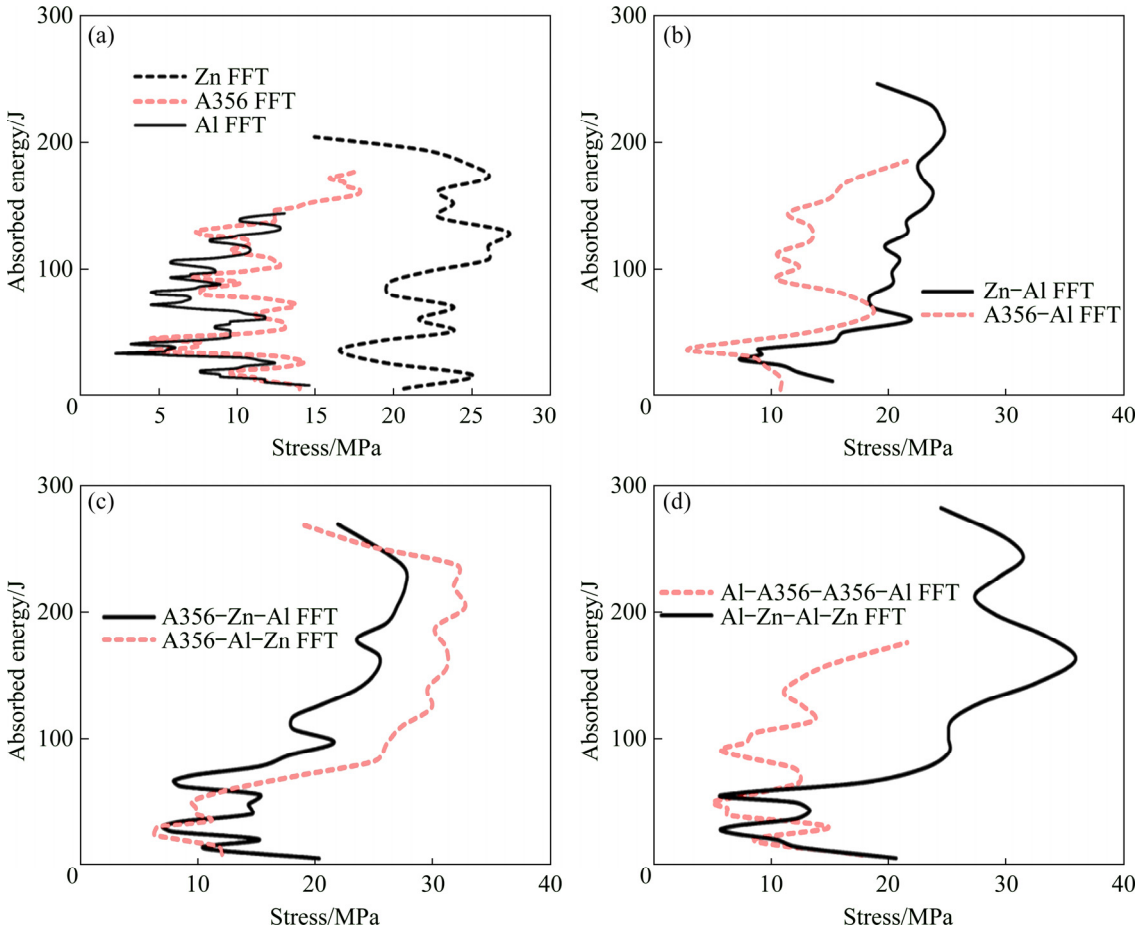

Fig. 14 Absorbed energy against stress during plastic deformation of some single-layer (a), double-layer (b), triple-layer (c) and quad-layer (d) structures under impact loading

plateau, greater interaction between the tube and foam fillers, more material interfaces and higher plastic energy damping in their layer style [32,68].

Figure 16 shows the effect of design parameters, including the density, material and number of foam layers on the average SEA of FGFTs. Figure 16(a) induces that the double-layer Al−A356 FFTs are of graded structures with the maximum average SEA of 10.4 J/g. On average, higher SEA values are obtained in the triple-layer FFTs with a smaller volume fraction of the zinc foam in contrast to the double- and quad-layer A356−Zn or Al−Zn FFTs. Consequently, the use of A356 alloy and aluminum foams improves the SEA of graded structures. The zinc foam deteriorates the crash performance, although the high-strength zinc foam significantly affects the crushing response of graded structures. Meanwhile, the average SEA of multilayer A356−Zn and Al−Zn FFTs is improved with increasing the number of layers in connection with more material interfaces and greater energy dissipation through the stepwise hardening plateau [69,70]. Regarding Fig. 16(b), the increase in relative density leads to a linear decrease in the SEA with a relatively high R^2 of 0.8455. This is in accordance with the other reports on the energy absorption capacity of foam-filled structures [38−44]. It is worthwhile noting that the multilayer

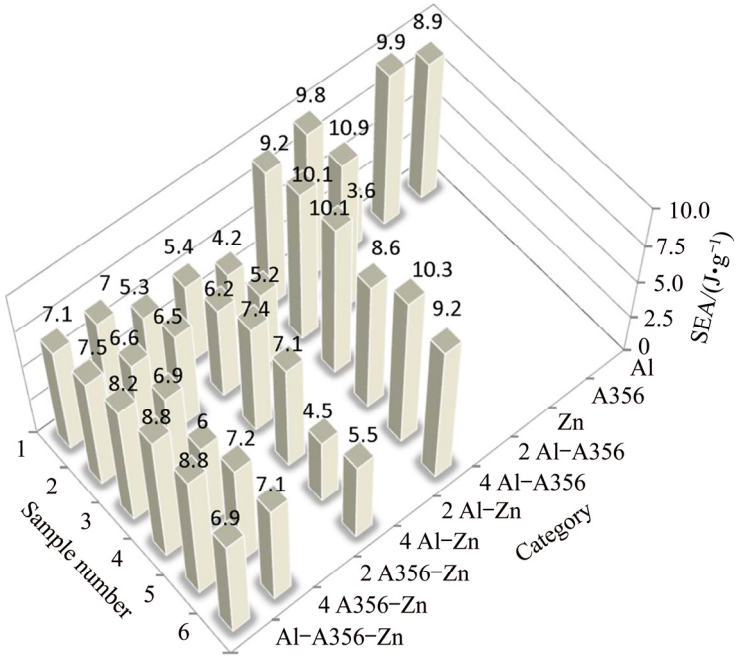

Fig. 15 SEA results from impact tests of FGFTs

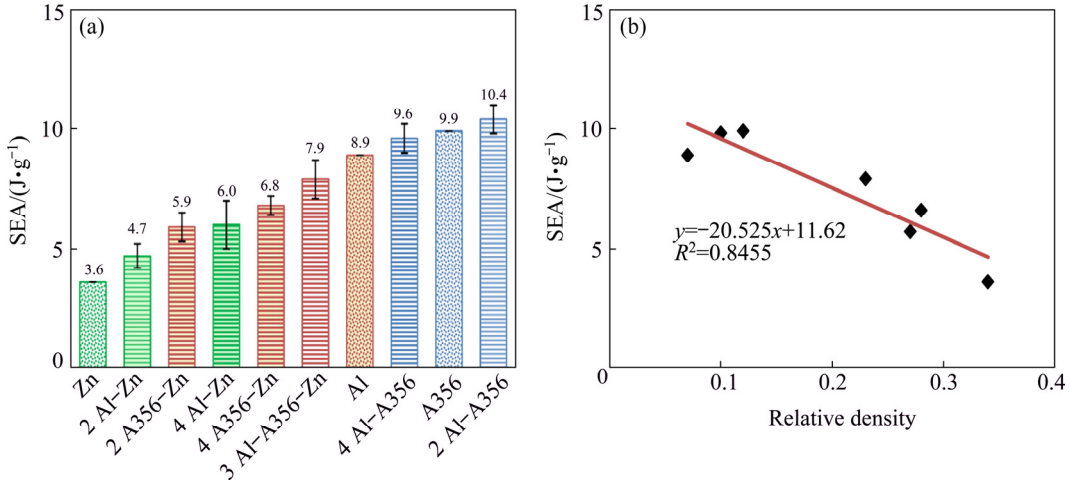

Fig. 16 Average SEA of FGFTs by varying material and number of foam layers (a), and relative density of graded foam fillers (b)

Al−A356 FFTs show a combination of the maximum SEA (10 J/g) and minimum σ_{peak} (10.2 MPa) among the proposed FGFTs (see Figs. 10, 15 and 16); thereby, they can be introduced as the best lightweight crashworthy structures. It can be concluded that the multilayer structures show overall superior crash performance to the uniform counterparts. Also, the density and material of foam layers are the most important parameters affecting the SEA of FGFTs.

4 Conclusions

(1) The multilayer FFTs reveal the multiple dynamic response and stepwise increment of stress as a consequence of plastic collapse of individual foam layers, initiating from the low-strength component.

(2) The A356 alloy foam is the best material for the improvement of SEA owing to its low density and great inherent strength, followed by the aluminum foam. The double-layer A356−Al FFT exhibits the maximum SEA of 10.9 J/g, which is 10% and 22% higher than that of the A356 FFT and Al FFT counterparts, respectively.

(3) The use of zinc foam causes a sharp increase in dynamic stress of FGFTs, although it has no positive effect on the crash performance and lowers the SEA. The mechanical properties and energy absorption capability of the graded structures are mostly dominated by the density and material of foam layers.

(4) The graded structures composed of the aluminum and A356 alloy foams deform in a symmetric mode under quasi-static and impact loadings, whereas the zinc foam leads to a combination of symmetric and extension modes. The dynamic and quasi-static collapse behaviors are distinguished by greater localized deformation and greater local rupture in the presence of zinc foam, respectively.

(5) The multilayer FFTs show overall superior crashworthiness to the uniform components, and the Al–A356 FFTs with a combination of the maximum SEA (10 J/g) and minimum σ_{max} (10.2 MPa) can be introduced as the best lightweight crashworthy structures.

Acknowledgments

This work was supported by the Metal Foam Group of Amirkabir University (MFGAU) through Grant No. 110-mir-13990531. The authors are grateful to Nowin Rahyaft Advanced Sciences and Technologies Knowledge Based Company for their support in casting and cutting the metal foams.

References

[1] VESENJAK M, SULONG M A, OPARA L K, BOROVINSEK M, MATHIER V, FIEDLER T. Dynamic compression of aluminium foam derived from infiltration casting of salt dough [J]. Mechanics of Materials, 2016, 93: 96−108.

[2] XIAO Li-jun, SONG Wei-dong. Additively-manufactured functionally graded Ti−6Al−4V lattice structures with high strength under static and dynamic loading: Experiments [J]. International Journal of Impact Engineering, 2018, 111: 255−272.

[3] ORBULOV I N, SZLANCSIK A, KEMENY A, KINCSES D. Compressive mechanical properties of low-cost, aluminium matrix syntactic foams [J]. Composites Part A, 2020, 135: 105923.

[4] KADER M A, ISLAM M A, SAADATFAR M, HAZELL P J, BROWN A D, AHMED S, ESCOBEDO J P. Macro and micro collapse mechanisms of closed-cell aluminium foams during quasi-static compression [J]. Materials and Design, 2017, 118: 11−21.

[5] LI M, LI J, BARBAT S, BACCOUCHE R, LU W. Enhanced filler-tube wall interaction in liquid nanofoam-filled thin-walled tubes [J]. Composite Structures, 2018, 200: 120−126.

[6] GOEL M D. Deformation, energy absorption and crushing behavior of single-, double- and multi-wall foam filled square and circular tubes [J]. Thin-Walled Structures, 2015, 90: 1−11.

[7] MOHAMMADIHA O, GHARIBLU H. Crush behavior optimization of multi-tubes filled by functionally graded foam [J]. Thin Walled Structures, 2016, 98: 627−639.

[8] ATTURAN U A, NANDAM S H, MURTY B S, SANKARAN S. Deformation behaviour of in-situ TiB2 reinforce A357 aluminium alloy composite foams under compressive and impact loading [J]. Materials Science and Engineering A, 2017, 684: 178−185.

[9] GERAMIPOUR, T. OVEISI H. Effects of foaming parameters on microstructure and compressive properties of aluminum foams produced by powder metallurgy method [J]. Transactions of Nonferrous Metals Society of China, 2017, 27: 1569−1579.

[10] ISLAM M A, KADER M A, HAZELL P J, ESCOBEDO J P, BROWN A D, SAADTFAR M. Effects of impactor shape on the deformation and energy absorption of closed cell aluminium foams under low velocity impact [J]. Materials and Design, 2020, 191: 108599.

[11] KADER M A, BROWN A D, HAZELL P J, ROBINS V, ESCOBEDO J P, SAADTFAR M. Geometrical and topological evolution of a closed-cell aluminium foam subject to drop-weight impact: An X-ray tomography study [J]. International Journal of Impact Engineering, 2020, 139: 103510.

[12] RAJAK D K, MAHAJAN N N, LINUL E. Crashworthiness performance and microstructural characteristics of foam-filled thin-walled tubes under diverse strain rate [J]. Journal of Alloys and Compounds, 2019, 775: 675−689.

[13] SAHU S, MONDAL D P, CHO J U, GOEL M D, ANSARI M Z. Low-velocity impact characteristics of closed cell AA2014−SiC_P composite foam [J]. Composites Part B, 2019, 160: 394−401.

[14] SUN Y, LI Q M. Dynamic compressive behaviour of cellular materials: A review of phenomenon, mechanism and modeling [J]. International Journal of Impact Engineering, 2018, 112: 74−115.

[15] BAROUTAJI A, SAJJIA M, OLABI A G. On the crashworthiness performance of thin-walled energy absorbers: Recent advances and future developments [J]. Thin-Walled Structures, 2017, 118: 137−163.

[16] ASTARAIE A H, SHAHVERDI H R, ELAHI S H. Compressive behavior of Zn−22Al closed-cell foams under uniaxial quasi-static loading [J]. Transactions of Nonferrous Metals Society of China, 2014, 24: 162−169.

[17] HUANG R X, MA S Q, ZHANG M D, XU J J, WANG Z Y. Dynamic deformation and failure process of quasi-closed-cell aluminum foam manufactured by direct foaming technique [J]. Materials Science and Engineering A, 2019, 756: 302−313.

[18] MYERS K, KATONA B, CORTES P, ORBULOV I N. Quasi-static and high strain rate response of aluminum matrix syntactic foams under compression [J]. Composites Part A, 2015, 79: 82−91.

[19] KADER M A, ISLAM M A, HAZELL P J, ESCOBEDO J P, SAADATFAR M, BROWN A D, THOMAS G J A. Modelling and characterization of cell collapse in aluminium foams during dynamic loading [J]. International Journal of Impact Engineering, 2016, 96: 78−88.

[20] LINUL E, MOVAHEDI N, MARSAVINA L. The temperature effect on the axial quasi-static compressive behavior of ex-situ aluminum foam-filled tubes [J]. Composite Structures, 2017, 180: 709−722.

[21] MOVAHEDI N, MURCH G E, BELOVA I E, FIEDLER T. Manufacturing and compressive properties of tube-filled metal syntactic foams [J]. Journal of Alloys and Compounds, 2020, 822: 153465.

[22] LINUL L, MOVAHEDI N, MARSAVINA L. On the lateral compressive behavior of empty and ex-situ aluminum foam-filled tubes at high temperature [J]. Materials, 2018, 11: 1−7.

[23] DIRGANTARA T, JUSUF A, KURNIATI E O, GUNAWAN L, PUTRA I S. Crashworthiness analysis of foam-filled square column considering strain rate effect of the foam [J]. Thin-Walled Structures, 2018, 129: 365−380.

[24] ZHANG Chun-ji, FENG Yi, ZHANG Xue-bin. Mechanical properties and energy absorption properties of aluminum foam-filled square tubes [J]. Transactions of Nonferrous Metals Society of China, 2010, 20: 1380−1386.

[25] ZHANG Y, LU M H, SUN G Y, LI G Y, LI Q. On functionally graded composite structures for crashworthiness [J]. Composite Structures, 2015, 132: 393−405.

[26] HANGAI Y, TAKASHI K, YAMAGUCHI R, UTSUNOMIYA T, KITAHARA S, KUWAZURU O, YOSHIKAWA N. Nondestructive observation of pore structure deformation behavior of functionally graded aluminum foam by X-ray computed tomography [J]. Materials Science and Engineering A, 2012, 556: 678−684.

[27] KIERNAN S, CUI L, GILCHRIST M D. Propagation of a stress wave through a virtual functionally graded foam [J]. International Journal of Non-Linear Mechanics, 2009, 44: 456−468.

[28] HE Si-yuan, LV Yi-nan, CHEN Shi-ting, DAI Ge, LIU Gia-gui, HUO Meng-ke. Gradient regulation and compressive properties of density-graded aluminum foam [J]. Materials Science and Engineering A, 2020, 772: 138658.

[29] HANGAI Y, TAKAHASHI K, UTSUNOMIYA T, KITAHARA S, KUWAZURU O, YOSHIKAWA N. Fabrication of functionally graded aluminum foam using aluminum alloy die casting by friction stir processing [J]. Materials Science and Engineering A, 2012, 534: 716−719.

[30] ZHANG X, ZHANG H. Optimal design of functionally graded foam material under impact loading [J]. Materials and Design, 2016, 102: 99−211.

[31] MOVAHEDI N, CONWAY S, BELOVA I V, MURCH G E, FIEDLER T. Influence of particle arrangement on the compression of functionally graded metal syntactic foams [J]. Materials Science and Engineering A, 2019, 764: 1−9.

[32] KOOHBOR B, KIDANE A. Design optimization of continuously and discretely graded foam materials for efficient energy absorption [J]. Materials and Design, 2016, 102: 151−161.

[33] MAHEO L, VIOT P. Impact on multi-layered polypropylene foams [J]. International Journal of Impact Engineering, 2013, 53: 84−93.

[34] MOVAHEDI N, MURCH G E, BELOVA I E, FIEDLER T. Functionally graded metal syntactic foam: Fabrication and mechanical properties [J]. Materials and Design, 2019, 168: 107652.

[35] HANGAI Y, KUBOTA N, UTSUNOMIYA T, KAWASHIMA H, KUWAZURU O, YOSHIKAWA N. Drop weight impact behavior of functionally graded aluminum foam consisting of A1050 and A6061 aluminum alloys [J]. Materials Science and Engineering A, 2015, 639: 597−603.

[36] HANGAI Y, SAITO K, UTSUNOMIYA T, KUWAZURU O, YOSHIKAWA N. Fabrication and compression properties of functionally graded foam with uniform pore structures consisting of dissimilar A1050 and A6061 aluminum alloys [J]. Materials Science and Engineering A, 2014, 613: 163−170.

[37] HANGAI Y, MORITA T, UTSUNOMIYA T. Functionally graded aluminum foam consisting of dissimilar aluminum alloys fabricated by sintering and dissolution process [J]. Materials Science and Engineering A, 2017, 696: 544−551.

[38] ZHANG J H, CHEN L, WU H, FANG Q, ZHANG Y D. Experimental and mesoscopic investigation of double-layer aluminum foam under impact loading [J]. Composite Structures, 2020, 241: 110859.

[39] LI G Y, ZHANG Z H, SUN G Y, XU F X, HUANG X D. Crushing analysis and multiobjective optimization for functionally graded foam-filled tubes under multiple load cases [J]. International Journal of Mechanical Sciences, 2014, 89: 439−452.

[40] YIN H F, WEN G L, HOU S J, QING Q X. Multiobjective crashworthiness optimization of functionally lateral graded

foam-filled tubes [J]. Materials and Design, 2013, 44: 414−428.

[41] YU X H, QIN Q H, ZHANG J X, HE S Y, XIANG C P, WANG M S, WANG T J. Crushing and energy absorption of density- graded foam-filled square columns: Experimental and theoretical investigations [J]. Composite Structures, 2018, 201: 423−433.

[42] ZHANG Yi, HE Si-yuan, LIU Jia-gui, ZHAO Wei, GONG Xiao-lu, YU Jin. Density gradient tailoring of aluminum foam-filled tube [J]. Composite Structures, 2019, 220: 451−459.

[43] SALEHI M, MIRBAGHERI S M H, ARABKOHI M. Compressive and energy absorption behavior of multilayered foam filled tubes [J]. Metallurgical and Materials Transactions A, 2019, 50: 5494−5509.

[44] MOVAHEDI N, MIRBAGHERI S M H, HOSSEINI S R. Effect of foaming temperature on the mechanical properties of produced closed-cell A356 aluminum foams with melting method [J]. Metals and Materials International, 2014, 20: 757−763.

[45] ISO 17340. Metallic materials, ductility testing, high speed compression test for porous and cellular metals [S]. 2014.

[46] ISO 13314. Mechanical testing of metals, ductility testing, compression test for porous and cellular metals [S]. 2011.

[47] FANG J G, GAO Y K, AN X Z, SUN G Y, CHEN J N, LI Q. Design of transversely-graded foam and wall thickness structures for crashworthiness criteria [J]. Composites Part B, 2016, 92: 338−349.

[48] ATTIA M S, MEGUID S A, NOURAIE H. Nonlinear finite element analysis of the crush behavior of functionally graded foam-filled columns [J]. Finite Element in Analysis and Design, 2012, 61: 50−59.

[49] LI Z B, CHEN R, LU F Y. Comparative analysis of crashworthiness of empty and foam filled thin walled tubes [J]. Thin-Walled Structures, 2018, 124: 343−349.

[50] YIN H F, WEN G L, FANG H B, QING Q X, KONG X Z, XIAO J R, LIU Z B. Multiobjective crashworthiness optimization design of functionally graded foam-filled tapered tube based on dynamic ensemble metamodel [J]. Materials and Design, 2014, 55: 747−757.

[51] ZHU G, LI S F, SUN G, LI G, LI Q. On design of graded honeycomb filler and tubal wall thickness for multiple load cases [J]. Thin-Walled Structures, 2016, 109: 377−389.

[52] SUN G Y, LIU T Y, HUANG X D, ZHENG G, Li Q. Topological configuration analysis and design for foam filled multi-cell tubes [J]. Engineering Structures, 2018, 155: 235−250.

[53] REZVANI M J, SOUZANGARZADEH H. Effects of triggering and polyurethane foam on energy absorption of thin walled circular tubes under the inversion process [J] Journal of Energy Storage, 2020, 27: 101071.

[54] SUN G Y, LI G Y, HOU S J, ZHOU S W, LI W, LI Q. Crashworthiness design for functionally graded foam-filled thin-walled structures [J]. Materials Science and Engineering A, 2010, 527: 1911−1919.

[55] FAN J H, ZHANG J J, WANG Z H, LI Z Q, ZHAO L M. Dynamic crushing behavior of random and functionally graded metal hollow sphere foams [J]. Materials Science and Engineering A, 2013, 561: 352−361.

[56] YANG X D, AN T, WU Z Q, ZOU T C, SONG H P, SHA J W, HE C N, ZHAO N Q. The effect of outer tube on quasi-static compression behavior of aluminum foam-filled tubes [J]. Composite Structures, 2020, 245: 112357.

[57] ZHOU X, LI Y X, CHEN X. Development of AlMg35−TiH_2 composite foaming agent and fabrication of small pore size aluminium foams [J]. Journal of Materials Processing Technology, 2020, 283: 116698.

[58] GIBSON L J, ASHBY M F. Cellular solids: Structure and properties [M]. 2nd ed. London: Cambridge University Press, 1997.

[59] YUAN Jian-yu, LI Yan-xiang. Effects of cell wall property on compressive performance of aluminum foams [J]. Transactions of Nonferrous Metals Society of China, 2015, 25: 1619−1625.

[60] JIANG Wen-ming, FAN Zi-tian, LIU De-jun. Microstructure, tensile properties and fractography of A356 alloy under as-cast and T6 obtained with expandable pattern shell ting process [J]. Transactions of Nonferrous Metals Society of China, 2012, 22: 7−13.

[61] ASM Handbook. Alloy phase diagrams [M]. 2nd ed. Ohio: ASM International, 1990.

[62] DIETER G E. Mechanical metallurgy [M]. 3rd ed. New York: McGraw-hill Education, 1986.

[63] LIU J A, YU S R, ZHU X Y, WEI M, LI S, LUO Y R, LIU Y H. Effect of Al_2O_3 short fiber on the compressive properties of Zn−22Al foams [J]. Materials Letters, 2008, 62: 3636−3638.

[64] GE C Q, GAO Q, WANG L M, HONG Z. Theoretical prediction and numerical analysis for axial crushing behaviour of elliptical aluminium foam-filled tube [J]. Thin-Walled Structures, 2020, 149: 106523.

[65] ZHANG Y, ZANG Xiao-yun, WANG Ke, HE Si-yuan, LIU Gia-gui, ZHAO Wei, GONG Xiao-lu, YU Jin. Fabrication of functionally radial graded metallic foam [J]. Materials Letters, 2020, 264: 127292.

[66] GUI M C, WANG D B, WU J J, YUAN G J, LI C G. Deformation and damping behaviors of foamed Al−Si−SiC_P composite [J]. Materials Science and Engineering A, 2000, 26: 282−288.

[67] DUARTE I, OPARA L K, VESENJAK M. Axial crush behaviour of the aluminium alloy in-situ foam filled tubes with very low wall thickness [J]. Composite Structures, 2018, 192: 184−192.

[68] GARDNER N, WANG E, SHUKLA A. Performance of functionally graded sandwich composite beams under shock wave loading [J]. Composite Structures, 2012, 94: 1755−1770.

[69] DUAN Y, ZHAO X H, LIU Z Y, HOU N D, LIU H F, DU B, HOU B, LI Y L. Dynamic response of additively manufactured graded foams [J]. Composites Part B, 2020, 183: 107630.

[70] DUAN Y, ZHAO X H, DU B, SHI X P, ZHAO H, HOU B, LI Y L. Quasi-static compressive behavior and constitutive model of graded foams [J]. International Journal of Mechanical Sciences, 2020, 177: 105603.

[71] HANSSEN A G, LANGSETH M, HOPPERSTAD O S. Static and dynamic crushing of square aluminium extrusions with aluminium foam filler [J]. International Journal of Impact Engineering, 2000, 24: 347−383.

功能梯度金属泡沫填充管在冲击载荷下的高效吸能

M. SALEHI, S. M. H. MIRBAGHERI, A. JAFARI RAMIANI

Department of Materials and Metallurgical Engineering, Amirkabir University of Technology, Tehran 15875-4413, Iran

摘　要：研究功能梯度泡沫填充管(FGFTs)在落锤冲击载荷作用下的变形行为和耐撞性。采用液态工艺制备的闭孔泡沫铝、A356 合金泡沫和锌泡沫作为轴向梯度填料，用于制备不同构造的单层和多层结构。结果表明，多层泡沫填充管的变形由低强度部位开始，然后通过应力的逐渐增加在高强度部位中扩展。使用更多的 A356 合金和泡沫铝层可为梯度结构提供更大的比吸能(SEA)，而高强度的锌泡沫对碰撞性能没有积极的影响。由泡沫铝和 A356 合金泡沫组成的梯度结构在准静态和落锤冲击条件下以对称模式发生连续倒塌。使用锌泡沫会引起对称模式和扩展模式倒塌，样品在动态加载下产生更大的局部变形，在准静态加载下产生更大的局部破裂。Al−A356 泡沫填充管具有最高的 SEA (10 J/g)和最低的初始峰值应力(σ_{max}=10.2 MPa)，是最好的轻质耐撞结构。

关键词：功能梯度泡沫填充管；落锤冲击；变形行为；比吸能；耐撞性

(Edited by Bing YANG)